Graphene Oxide: Structural Analysis and Application as a Highly Transparent Support for Electron Microscopy

Neil R. Wilson,[†,*] Priyanka A. Pandey,[†] Richard Beanland,[†] Robert J. Young,[§] Ian A. Kinloch,[§] Lei Gong,[§] Zheng Liu,[⊥] Kazu Suenaga,[⊥] Jonathan P. Rourke,[‡] Stephen J. York,[†] and Jeremy Sloan[†,*]

[†]Department of Physics, University of Warwick, Coventry CV4 7AL, U.K., [‡]Department of Chemistry, University of Warwick, Coventry CV4 7AL, U.K., [§]School of Materials, The University of Manchester, Grosvenor Street, Manchester M1 7HS, U.K., and [⊥]National Institute of Advanced Industrial Science and Technology (AIST), Research Centre for Advanced Carbon Materials, Tsukuba, Ibaraki 3058565, Japan

ABSTRACT We report on the structural analysis of graphene oxide (GO) by transmission electron microscopy (TEM). Electron diffraction shows that on average the underlying carbon lattice maintains the order and lattice-spacings of graphene; a structure that is clearly resolved in 80 kV aberration-corrected atomic resolution TEM images. These results also reveal that single GO sheets are highly electron transparent and stable in the electron beam, and hence ideal support films for the study of nanoparticles and macromolecules by TEM. We demonstrate this through the structural analysis of physiological ferritin, an iron-storage protein.

KEYWORDS: graphene oxide · graphite oxide · ferritin · structural analysis · high resolution electron microscopy · electron diffraction · Raman spectroscopy

The electronic and mechanical properties of graphene sheets, single atomic layers of carbon arranged in a hexagonal lattice, are undoubtedly extraordinary,[1] but their fabrication is challenging.[2] High quality single graphene sheets can be prepared by mechanical exfoliation of graphite, which is laborious, has a low yield,[3] and is unlikely to be a good route for commercially viable devices. Thus a concerted effort is now in progress to find an economic and scalable fabrication route which will allow graphene to be exploited more fully.[2] Techniques which could be used on a commercial scale include graphitization of SiC,[4] patterned chemical vapor deposition onto Ni layers,[5] and the reduction of graphene oxide (GO)—single sheets of carbon with a mixture of carboxyl, epoxy and/or hydroxyl functionalities—into chemically converted graphene (CCG).[6−8] In terms of commercial scalability, GO is the most promising of these as it can be prepared in large-scale quantities as hydrophilic graphene-like monolayers and is dispersible in aqueous media, making it easier to handle, functionalize, transport, and deposit than native graphene. GO is also an example of, and the usual precursor to, chemically modified graphene (CMG), graphene sheets modified by functional groups or macromolecules to control electronic, optical, or mechanical properties[2,9] for applications such as enhanced polymer nanocomposites.[10]

Oxidized graphite, graphitic oxide, has been known for over a hundred years[11] but its structure is still not precisely determined; it has variable stoichiometry, and the local arrangement of functional groups—and how their configurations vary with the degree of oxidation or reduction—is unclear. GO is usually derived from the exfoliation of graphitic oxide, and hence is likely to share a similar structure. GO has intriguing physical characteristics, being an insulator/semiconductor with conductivity strongly dependent on the degree of oxidation or reduction,[7] and electron energy-loss spectroscopy (EELS) investigations show that it has an electronic structure distinct from both graphene and amorphous carbon.[12] Some recent reports have suggested GO is amorphous or semiamorphous,[8,12−14] but it has been known for over 40 years from transmission electron microscopy (TEM) studies that the closely related material graphitic oxide retains strong crystalline order.[15−18] Here, we use TEM imaging and diffraction to demonstrate that this is also true of GO. Furthermore, we show that the interatomic spacing in GO is, to an accuracy of better than 0.5%, identical to that of graphene. Using spherical aberration-corrected high resolution TEM (HR-TEM) at 80 kV we are able to obtain atomically resolved images of GO, and show that it retains a graphene-like lattice substructure; in combination these results allow us to eliminate several recently proposed structural models.

*Address correspondence to J.Sloan@warwick.ac.uk, Neil.Wilson@warwick.ac.uk.

Received for review May 12, 2009 and accepted August 12, 2009.

Published online August 18, 2009.
10.1021/nn900694t CCC: $40.75

Like graphene, GO is highly electron transparent due to its low atomic number and two-dimensional nature. As a result, graphene and GO have obvious applications in TEM not only as objects of study in themselves, but also as a nearly perfect support film for other nanoparticles and macromolecules. To date, 1.6 nm carbon films from decomposition of self-assembled monolayers[19] and graphene[20,21] have been used as ultrathin support films, allowing images of single heavy metal atoms to be obtained. Again, the difficulty in production of single graphene layers,[22,23] especially in a geometry compatible with their use as a TEM support, means that their routine use is unlikely. Here, we demonstrate that GO is an extremely effective ultrathin TEM support film: it is stable in the electron beam, gives low background in both imaging and diffraction modes, and can also serve as its own calibration standard. Importantly, GO ultrathin support films are simple, cheap, and quick to fabricate in any laboratory, and as a result we expect they will find widespread application in the immediate future.

Our interest in the structure of GO thus has two aspects: that of the material in itself and the implications for its use as a route to CCG and CMG; and the underlying structure present when used as a support film for other nanostructures.

RESULTS AND DISCUSSION

Synthesis and Characterization of Graphene Oxide. Aqueous suspensions of GO were prepared *via* a modified Hummers method;[24,25] details of the process are given in the experimental section. A photograph of GO suspensions of decreasing concentration is shown in Figure 1a. The brown color is characteristic of highly oxidized GO, and its clarity indicates the GO is fully suspended. X-ray diffraction of a thin-film formed by vacuum filtration of the GO suspension revealed an interlayer separation of 0.85 nm with no graphite-like peak remaining, consistent with the complete oxidation of the graphite powder precursor.[26] Thermogravimmetric analysis (TGA) in air, the solid line in Figure 1b, reveals a mass loss at around 200 °C which has previously been assigned to removal of the functional groups.[18] This is also evident in an Ar/H_2 environment, the dashed line in Figure 1b, while the second mass loss at around 600 °C which has been assigned to burning of the carbon is not. By comparison TGA of the graphite powder precursor, the red line in Figure 1b, shows no weight loss until the temperature exceeds 700 °C. The GO weight loss below 200 °C has been assigned to water, and must be considered when evaluating the composition derived from elemental analysis.[18] Combining this TGA and elemental analysis we find a C:O ratio for our samples of roughly 2:1, which is consistent with previous reports and the approximate chemical formula for fully oxidized graphite oxide of $C_4O(OH)$ which dates back more than 40 years.[16]

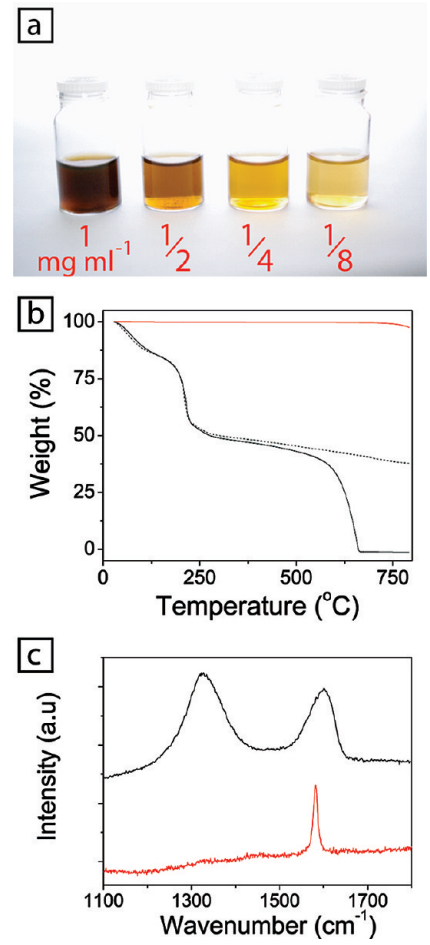

Figure 1. (a) Photograph of aqueous graphene oxide suspensions of decreasing concentration from left to right as marked. (b) TGA of graphite powder in air (red line), graphene oxide in air (solid black line), and graphene oxide in Ar/H_2 (dashed line). (c) Raman spectra of monolayer graphene oxide (black line) and monolayer graphene (red line).

Raman spectroscopy has been used extensively to probe the degree of disorder in graphite-like materials.[27] Figure 1c shows the micro-Raman spectra in the region 1100−1800 cm^{-1} for monolayer graphene, red line, and monolayer GO, the black line which is offset for clarity, both on silicon oxide. The spectra were taken using a 633 nm HeNe laser. As expected, graphene shows a single sharp peak at 1580 cm^{-1}, the G band characteristic of three-coordinate planar ("sp^2-hybridized") carbon. GO shows a broadened and blue-shifted G band at 1590 cm^{-1} and a broad, intense peak at 1330 cm^{-1}, the disorder-induced D band. The blue-shifted, broadened G band and intense D band are consistent with previous Raman investigations of GO[28] and are indicative of the severe disruption or disorder induced into the sp^2 carbon lattice by the oxidative synthesis of GO. To study this further we apply transmission electron microscopy to investigate the physical structure of the underlying carbon lattice in GO.

Structural Analysis of GO. For TEM analysis a drop of GO was deposited on a conventional lacey carbon sup-

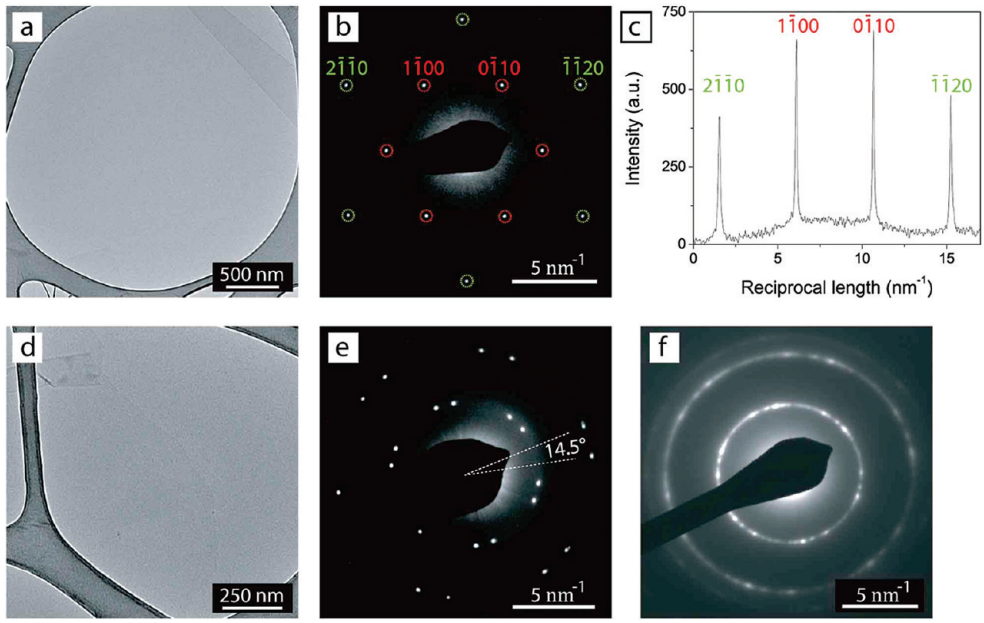

Figure 2. (a) TEM image of a single GO sheet on a lacey carbon support; a double fold is visible in the top right corner. (b) SAED of the center of the region shown in panel a, the diffraction spots are labeled with Miller−Bravais indices. (c) Intensity profile through the diffraction spots labeled in panel b. (d) TEM image with two overlapping GO sheets; a SAED pattern from the double sheet region (lower left side) is given in panel e. (f) Electron diffraction pattern from a thin film of GO *ca.* 15−20 layers thick.

port.[29] As is evident in Figure 2a, a low magnification TEM image, GO is highly electron transparent even in comparison to the thin-film carbon support. In the top right of the image a double fold in the sheet is visible; the contrast here is due to three layers. A selected area electron diffraction (SAED) pattern from the monolayer region of the GO film is shown in Figure 2b. Strikingly, clear diffraction spots are observed characteristic of crystalline order; the 6-fold pattern is consistent with a hexagonal lattice and the spots are labeled accordingly using Miller−Bravais *hkil* notation.

This simple hexagonal pattern of sharp spots is similar to those obtained from graphite oxide[15−17] and leads immediately to several conclusions. First, the GO sheets are not completely amorphous; sharp spots indicate short-range order over a length scale of the coherence length of the electron beam, which is a few nm under the conditions used here. Second, long-range orientational order is present, which extends at least as far as the width of the selected area aperture (*ca.* 0.6 μm), since any rotation of the sheet would appear as smearing or splitting of the spots. In fact it was possible to obtain similar SAED patterns from regions several μm in size, indicating that each comparable sheet is essentially "single crystal". Third, the lack of any diffraction spots other than those corresponding to the graphite structure shows that any oxygen-containing functional groups present (of which the GO must partly comprise) do not form superlattice-type ordered arrays.

The symmetry of the diffraction pattern alone does not prove the presence of GO rather than graphite oxide, that is, single sheet rather than graphite-like ordered multilayers. It has been shown by Meyer *et al.*[30] that the relative intensities of the $1\bar{1}00$-type and $2\bar{1}\bar{1}0$-type reflections and their behavior with specimen tilt can be used to distinguish between single-sheet graphene and few-layer graphite. In fact, any A−B stacked graphene-like structure thicker than one monolayer will give higher diffracted intensities for $21\bar{1}0$-type spots than $1\bar{1}00$-type spots because of interference between electrons scattered from the A-type and B-type layers.[16,30−32] This is a general result, and is independent of the atomic species or occupancy of the two different sites. For our material, Figure 1c shows that the inner $1\bar{1}00$-type reflections, marked by red dotted circles, are more intense than the outer $2\bar{1}\bar{1}0$-type reflections, marked in green, that is, are consistent with single layer rather than multilayers. Furthermore, AFM investigations of GO spin-cast on SiO_2 showed that the sheets were 0.8−1.5 nm thick, a result consistent with previous observations of single sheet GO[6,7,33] (see Supporting Information).

Averaged over all equivalent spots, the $1\bar{1}00$-type reflections in Figure 2b are roughly twice as intense as $2\bar{1}\bar{1}0$-type reflections; similar intensity ratios were found in all single GO sheets examined. This is significantly higher than the intensity ratio of 1.1:1 predicted for graphene,[32] but is consistent with other observations of oxidized carbon nanofilms.[32]

In Figure 2d, a hole in the lacey carbon support is covered by one graphene sheet with an overlapping sheet clearly visible on the left. The edge of this second sheet is rough, consistent with recent observations

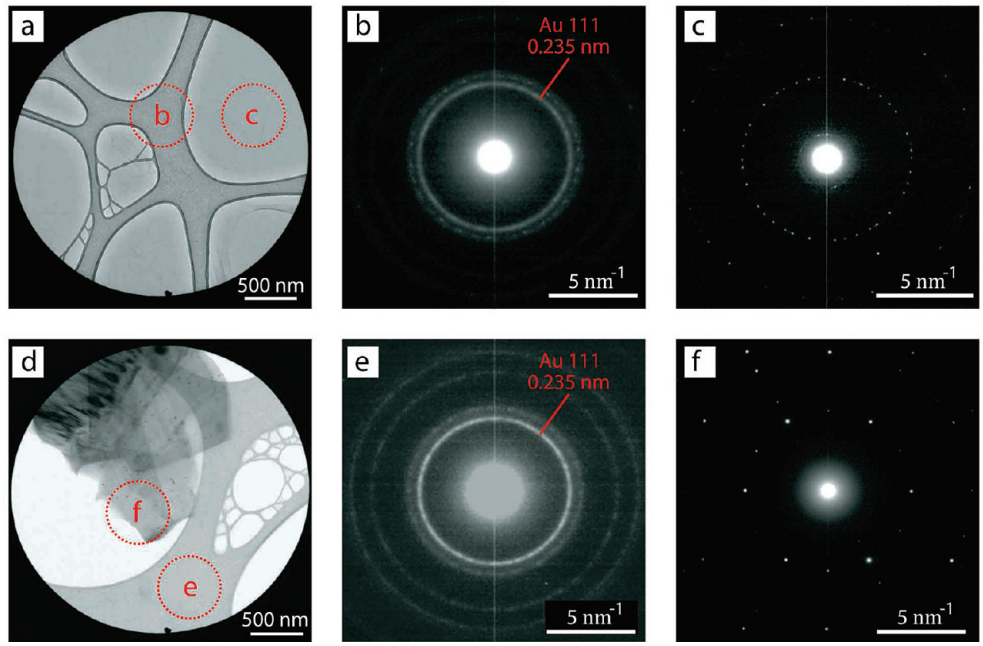

Figure 3. (a) TEM image of multiple GO sheets on a gold-coated lacey carbon support; (b,c) SAED patterns from the regions marked accordingly in panel a. The dominant features in panel b are rings characteristic of polycrystalline gold, which are used to calibrate the GO pattern (*ca.* 7 overlapping sheets) in panel c. (d) TEM image of few-layer graphite on a gold coated lacey carbon support; (e,f) SAED patterns from the regions marked accordingly in panel d. The gold diffraction pattern in panel e is used to calibrate the pattern due to few-layer graphite in panel f.

of thermally treated graphite.[34] The SAED pattern from the double sheet region, Figure 2e, is a superposition of two hexagonal patterns rotated by 14.5°. This angle corresponds to a misorientation between two individual GO sheets; an effect also observed recently in few-layer graphene samples.[35] We have studied many multilayer regions, but have not observed any preferred orientational relationships between the overlapping sheets. The orientation of the graphene-like GO sheet can be slightly different either side of a fold, as in the top right of Figure 2a, so single sheets can result in a multiple spot pattern; but multiple sheets have always been observed to give multiple spot patterns. Figure 2f shows a diffraction pattern produced from a film of GO, *ca.* 15−20 layers thick, formed by vacuum filtration. Individual spots are now barely visible as the contributing patterns merge into a ring pattern characteristic of a polycrystalline sample. This suggests that there are no preferred stacking orientations between the GO monolayers when the thin film is formed in this way, a result that may be significant for understanding electrical transport within them.

Accurate interplanar spacings (*d*-spacings) can also be extracted from electron diffraction patterns when careful attention is paid to experimental parameters. Variations in specimen height in the objective lens, as well as projector lens distortions and astigmatism, introduce errors of several percent into uncalibrated measurements of *d*-spacings in SAED patterns, even on calibrated microscopes. However, by depositing a thin Au layer on the lacey carbon film before drop-casting of GO, we were able to correct for these distortions and calibrate the patterns to a precision better than 0.5% (see Supporting Information). Figure 3a is a low magnification image of GO on Au-coated lacey carbon; Figure 3b shows a SAED pattern from a region containing Au, GO, and amorphous carbon. Since the GO is very thin, and the carbon support amorphous, the main features are the rings characteristic of polycrystalline Au; the innermost and strongest ring corresponds to diffraction from planes with a spacing of 0.2355 nm. This was used for calibration. Figure 3c shows a SAED pattern from the adjacent region, containing multiple GO sheets. Analysis of 10 similar regions across several samples gave a *d*-spacing for GO $1\bar{1}00$-type planes of 0.2131 ± 0.0010 nm. The variation between measurements was smaller than the experimental error (*ca.* 0.5%, limited by the accuracy with which the Au 111 ring could be measured), indicating that the GO structure does not vary significantly from place to place within samples, or between samples of different origin. This corresponds to an average, in-plane[36] carbon−carbon spacing (C−C spacing) of 0.1421 ± 0.0007 nm.

Few-layer graphite (FLG) samples were measured using the same procedure (Figures 3d−f), giving a value for $1\bar{1}00$-type planes of 0.2138 ± 0.0010 nm. The lattice parameter of GO and graphite are therefore identical within experimental error. The measured GO C−C spacing of 0.1421 ± 0.0007 nm agrees well with the accepted value for graphite of 0.142 nm; implying that the crystalline structure of GO is similar to graphene, that is, three-coordinate carbon atoms bound in a planar arrangement ("sp^2-hybridized").

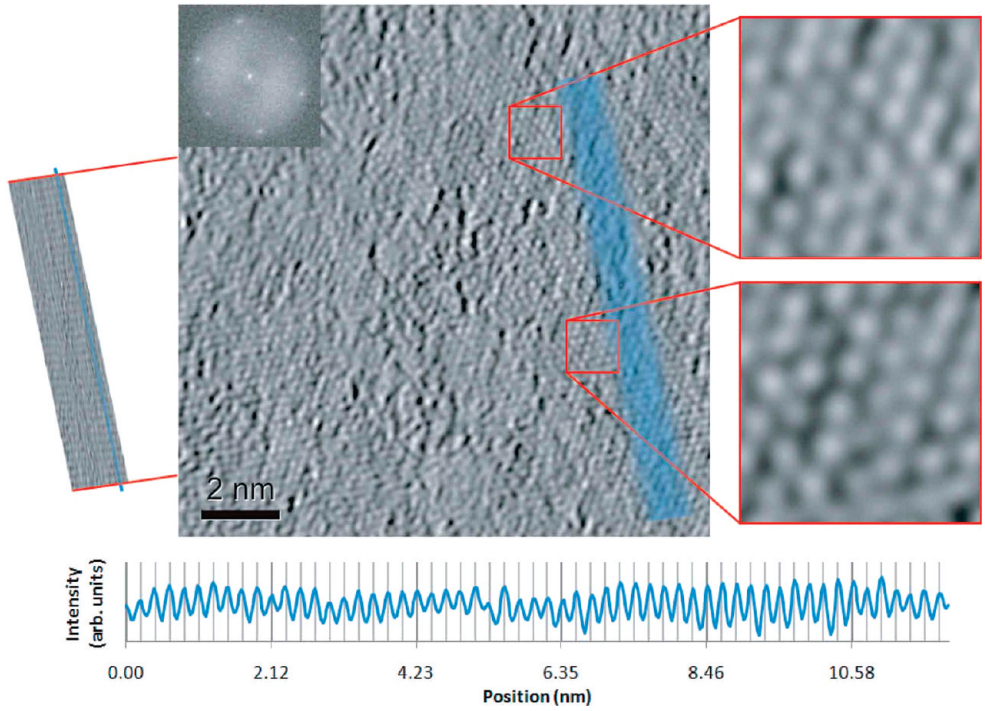

Figure 4. (Main panel) HR-TEM of a single sheet of GO, with an FFT of the image (inset top left); (right) enlargements as marked, showing the GO crystalline lattice; (left) digital compression of a portion of the image (to 10% of its width) along the direction marked by the red lines, the clearly visible parallel lines demonstrate the regular period of the lattice planes; (below) line plot of the average intensity along the blue line (marked on both compressed and original images), the gray lines are guides to the eye.

The observed C−C spacing does not exclude the presence of four-coordinate carbon atoms ("sp^3-hybridized") distributed in a random manner across the GO sheets; it simply shows that the crystalline carbon component of the structure present in single sheets of GO is predominantly the same as that of graphene. The change from planar sp^2 to tetrahedrally coordinated sp^3 carbon increases the carbon−carbon bond length (*e.g.*, in diamond it is 0.154 nm), and changes the bond angles so that for a single sheet of diamond-like carbon the C−C spacing would be 0.145 nm, that is, a net increase of 2% over graphene. This would be well within our detection limits, and was recently observed for hydrogenated graphene, or graphane.[37] Boukhvalov and Katsnelson modeled the effect of oxygen and hydroxyl groups on the structure of graphene oxide,[38] they predicted that the carbon−carbon bond length was highly dependent on the types of functional groups and their coverage. Unfortunately they did not include data on the bond angles so we cannot compare our results quantitatively to theirs; however, the precision of this electron diffraction analysis will enable direct comparison with theoretical structure predictions.

HR-TEM of GO. Diffraction patterns give information on the average crystal structure of a material but are not strongly affected by minor disorder or defect structures. HR-TEM images of the structure are much more useful in this respect; however, the electron flux is much higher than is the case for SAED (where a fully spread parallel beam is used) and damage occurs much more rapidly. It has been reported (see, for example, Zobelli *et al.*[39]) that crystalline carbon structures are significantly less affected in TEM by accelerating voltages lower than 100 kV. We therefore performed spherical aberration-corrected HR-TEM imaging at 80 kV in order to minimize damage to the local structure. Under these imaging conditions GO was indeed found to be highly stable; it was also stable for routine observation at higher accelerating voltages (see HR-TEM of ferritin below), although irradiation at high fluxes during high resolution imaging with intense electron sources did lead to eventual break-up of the GO sheet.

Figure 4 shows a single sheet of GO, as determined from inspection of the diffraction pattern and fast Fourier transform (FFT) of the image (inset). The GO crystalline lattice is clearly visible in many regions of the image, shown in the enlargements to the right, while in others it appears to be obscured by disordered material, the origin of which is unclear. In previous HR-TEM investigations of graphene, significant amounts of amorphous adsorbates were observed;[20,23,40] this is likely to be so-called adventitious carbon,[41] well-known to surface scientists, but may also be oxidized carbons formed as a result of the GO preparation,[24,25] or a mixture of both. Hence it is difficult at present to determine whether the disordered material is a property of the GO sheet, or of contaminants adsorbed onto it.

On the left in Figure 4, a portion of the image has been digitally compressed to 10% of its width along

the direction marked by the red lines: the clearly visible parallel lines demonstrate the regular period of the lattice planes. Below the main image, a line plot of the average intensity along the blue line (marked on both compressed and original images) is shown: the gray lines are guides to the eye and are spaced to match the GO lattice-spacing (*ca*. 0.212 nm according to the uncalibrated magnification of the microscope). It is clear that the lattice plane spacing is constant, demonstrating crystalline order of the underlying lattice over length-scales of >10 nm.

Conclusions on the Structural Analysis of GO. In summary, electron microscopy of GO produced by a modified Hummers method shows that (1) it on average maintains the hexagonal symmetry and order of an unmodified graphene sheet; (2) it has an average in-plane carbon−carbon spacing of 0.1421 ± 0.0007 nm, indistinguishable from that of graphene; (3) it has no regular ordering of the functional groups; (4) the underlying carbon lattice has hexagonal order on the length-scale of the coherence of the electron beam (a few nm), evident from diffraction patterns; a graphene-like lattice with crystalline order on length-scales >10 nm as visible by atomic-resolution HR-TEM; and long-range orientational order over the entire (typically micrometer size) GO sheet, as evident in the SAED patterns; (5) it has no preferential stacking arrangement between adjacent sheets when deposited by drop-casting.

The most prominent proposed structure models (reviewed by Szabo *et al.*[26]) for graphite oxide, which are also considered to be the most appropriate for GO, include (a) the Hofmann model (random epoxy groups on planar graphene); (b) the Ruess model (random hydroxl and epoxy functionalities on a puckered carbon template); (c) Scholz−Boehm (as Ruess but with hydroxyl and carbonyl functional groups); (d) Nakajima−Matsuo (as Scholz−Boehm but with electron delocalization on the C═O groups); and (e) the Lerf−Klinowski model (as Hofmann but with random hydroxyl and epoxy groups with layer −COOH terminations). Szabo *et al.*[26] proposed a further model (f) combining elements of several of these, including randomly distributed hydroxyl, epoxy, and carbonyl groups distributed over a folded carbon skeleton. Development of these models mainly relied on chemical analysis techniques such as nuclear magnetic resonance, infrared spectroscopy, and X-ray photoelectron spectroscopy, none of which give the structural information available through TEM. Of these, models b, c, d, and f would give diffraction patterns clearly inconsistent with those presented here, either due to lack of hexagonal symmetry, or the presence of significant regions with carbon sp^3 bonding which would reduce *d*-spacings or give extra spots in the SAED patterns due to an oxidized superstructure. Models a and e are similar, differing mainly in the type of functional groups present, and appear to be consistent with our observations.

In addition to shedding light on the structure of the carbon lattice in GO, these TEM investigations also demonstrate that GO is highly electron transparent and stable in the electron beam. This suggests its use as a support film for TEM, as a first demonstration of this we have investigated the iron-containing protein ferritin which has been studied by electron microscopy for over 50 years, and has been well established as a resolution test for both instruments and support films.[42,43]

GO as a Support Film: Diffraction and Imaging of Ferritin. Ferritin is a globular protein about 12 nm in diameter, composed of a protein shell consisting of 24 subunits which surround a *ca*. 6 nm diameter central cavity filled with a hydrated iron oxide nanocrystal. Its role in living organisms is to store iron in a nontoxic form, and observed changes in the structure of the ferritin core are associated with aging and some neuro-degenerative disorders.[44] As a result, the mineral phase of the ferritin core has been the subject of considerable attention since the 1960s;[42] the dominant candidate being so-called "six-line" ferrihydrite.[45,46] In common with GO, there is a poor consensus on the crystal structure of ferrihydrite,[45] principally due to the difficulties involved in structural analysis of nanoparticles of this size. X-ray diffraction is of limited use because of the Scherrer broadening effect associated with small particle size. In TEM, the diffuse background scattering of the support film usually obscures the weak diffraction from an individual nanoparticle. Similarly, HR-TEM imaging of the protein shell is obscured by contrast innate to the support films which also reduces the clarity with which the core can be observed. Broad suites of measurements have thus been required to collectively infer the core structures. For example, a recent work demonstrating that a magnetite-like phase becomes more prevalent as iron is removed from the ferritin core[47] required the correlation of TEM, X-ray absorption near edge spectroscopy (XANES), EELS, small-angle X-ray scattering (SAXS) and SQUID magnetic studies in order to determine the constituent phases. We show here that through the use of GO as a high-transparency support, this structural information is achievable through conventional electron diffraction and HR-TEM alone.

Figure 5a shows a low magnification image of a low density of ferritin dispersed on GO. The iron oxide core of the ferritin particles can be clearly resolved against the weak background of the GO sheet. In particular, the contrast between ferritin and GO is significantly higher than between ferritin and a lacey carbon support. A SAED pattern of a 600 nm region of GO with approximately 500 ferritin particles is shown in Figure 5b; spots from both the GO and the ferritin are evident—this is emphasized in Figure 5c where diffraction from ferritin is marked in red and that from GO in green. It is important to note that the ferritin spots are clearly visible in the SAED pattern due to the low background scattering intensity of the GO film, significantly

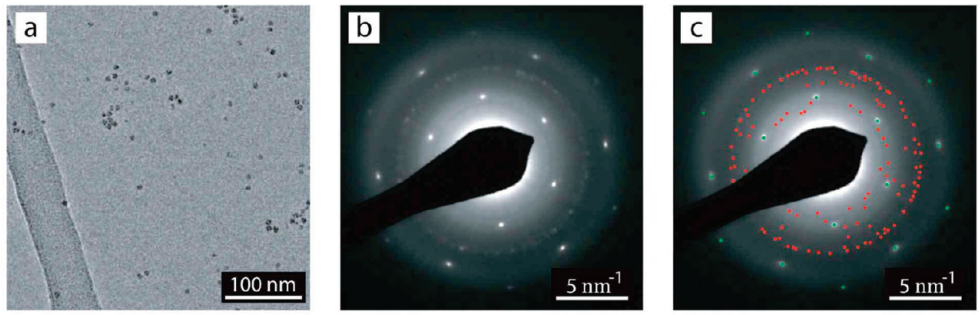

Figure 5. (a) TEM image of ferritin (dark particles) on GO. The lacey carbon support can be seen to the lower left. (b,c) SAED of a region containing *ca.* 500 particles on a single sheet of GO. More than 100 ferritin diffraction spots are visible, these are marked in panel c in red, with the spots due to GO marked in green.

lower than conventional thin carbon support films. The sharp spots from the GO are also an advantage; these can now be used as an internal calibration to enable accurate determination of the *d*-spacings in the ferritin core (see Supporting Information). A histogram of the ferritin core *d*-spacings after calibration is given in Figure 6, also marked are the spacings predicted for "six-line" ferrihydrite.[46] The correlation between the two is excellent, confirming that for this sample of ferritin the core composition is predominantly "six-line" ferrihydrite. Using GO as a low-background support it is thus possible to identify the dominant phase of the ferritin core using only conventional electron diffraction.

HR-TEM of Ferritin on GO. As described above for the structural analysis of GO, high resolution imaging is complementary to electron diffraction analysis in that it gives local structural information. In particular, it is possible to identify the phase of *individual* nanoparticle cores using HR-TEM. Figure 7a shows an idealized model of a ferritin molecule, with protein subunits surrounding a central 6 nm diameter ferrihydrite core, marked in orange. In the background, and to scale, is a graphene lattice.[48] The corresponding simulation, Figure 7b, used a standard multislice algorithm with parameters typical for this instrument (see Experimental Section) and was calculated for optimum Sherzer defocus conditions. The image contrast has three distinct components: (i) diffuse background contrast due to the graphene support; (ii) intermediate complex contrast due to the protein shell; and (iii) strong contrast due to the ferrihydrite core. For this particular core orientation[49] and imaging conditions the white spots in the core correspond to "oxygen tunnels"; these scatter less than the surrounding dark "honeycombed" lattice which also contains the denser iron; that is, in this [001] orientation the white spots correspond to atom-columns of oxygen.

A HR-TEM lattice image of ferritin on GO, Figure 7c, shows contrast due to two ferrihydrite particles of different sizes: particle 1, left, *ca.* 6 nm in diameter; and particle 2, right, *ca.* 3 nm in diameter. The core structure correlates well with the simulation in Figure 7b allowing identification of the white spots in the image as atom-columns of oxygen. Further evidence of the core composition comes from selected area FFTs: Figure 7 panels d and e are FFTs obtained from the marked regions containing particles 1 and 2, respectively. These are as expected for ferrihydrite particles with the same relative [001] orientation as used for the simulation, Figure 7b. It is thus possible from this HR-TEM image to not only measure the size and *d*-spacing of the nanoparticles, but also to identify their crystalline phase and orientation.[50]

The contrast of the material surrounding the particles is dominated by the complex contrast due to the protein shell and is significantly stronger than the supporting GO film. Under these imaging conditions (300 kV) this material will have been severely damaged by the electron beam, and hence no meaningful structural information can be extracted. However, due to the low background of the GO film the use of low dose imaging may allow investigation of the protein shell without prior staining, indicative of the potential use of GO support films for the study of biomaterials.

In summary, structural analysis of ferritin on GO has allowed the identification of the predominant core composition by electron diffraction, identification of

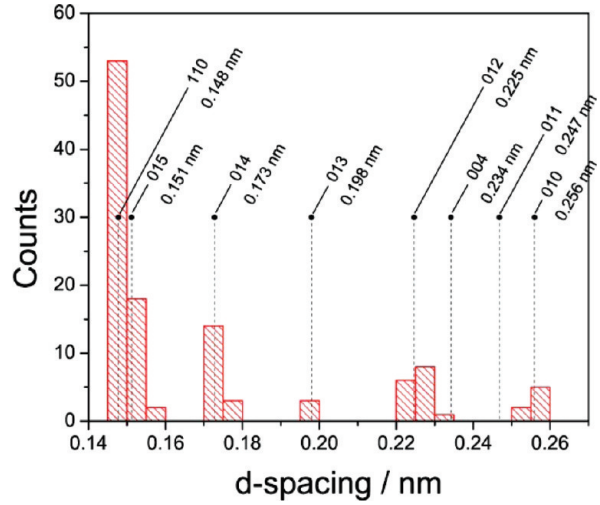

Figure 6. Histogram of the *d*-spacing of the ferritin diffraction peaks marked in Figure 5c after calibration. The dotted lines and labels (*hkl* and *d*-spacing) correspond to the peaks predicted for "six-line" ferrihydrite.

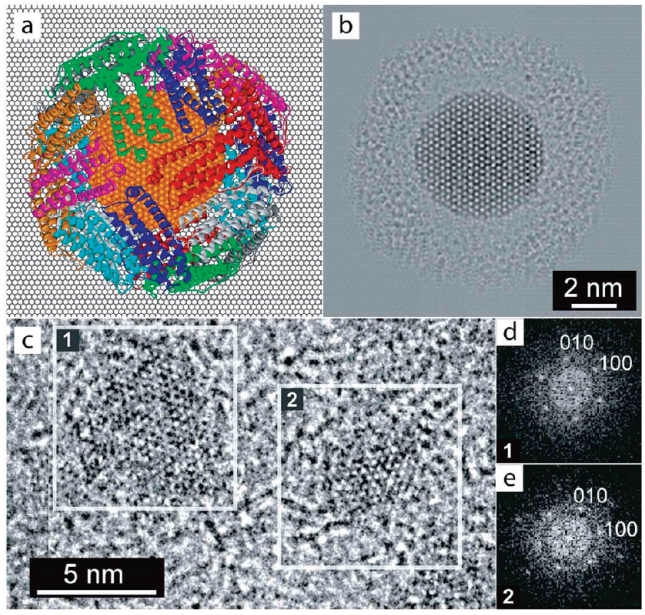

Figure 7. (a) Schematic model of ferritin on a graphene sheet. Ferritin consists of a protein shell (multicolored ribbons) containing a ferrihydrite core (Fe atoms indicated by orange spheres, O by red spheres) which here is oriented along [001] relative to the bulk crystal structure. (b) HRTEM image simulation of the structure in panel a. (c) 300 kV HRTEM image of ferritin on a single sheet graphene oxide support; (d,e) FFTs obtained from the marked regions 1 and 2, respectively, in panel c.

the core composition, and orientation by HR-TEM, and observation of the degraded protein shell. In particular we emphasize the ease with which they could be attained through the use of GO as a low background support. The ability to use the GO to accurately calibrate the diffraction pattern, without obscuring the pattern due to the nanoparticles, is another significant improvement over other approaches. Finally, it should be emphasized that in contrast to other ultrathin films, these GO support films are simple and quick to make—a drop of GO suspension is placed on an appropriate TEM grid and allowed to dry prior to the addition of the material to be studied. GO support films can be suspended directly onto standard TEM grids without the aid of lacey carbon films (see Supporting Information) creating large area GO films, and reducing the cost. Currently the yield for this is low as even the largest GO sheets in our preparation are smaller than the holes in standard TEM grids; however, this could be substantially improved using GO synthesis processes such as that reported by Luo *et al.*[33] which produced macroscopic sheets with sizes comparable to the hole size in 400 mesh TEM grids.

CONCLUSIONS

We have applied electron microscopy to the structural analysis of graphene oxide and made concrete observations against which structural models of graphene oxide must be tested. Most strikingly, the carbon substructure of graphene oxide is found on average to maintain the hexagonal symmetry, order, and carbon−carbon bond length of an unmodified graphene sheet. Atomic resolution HR-TEM reveals an underlying graphene-like lattice with crystalline order on length-scales >10 nm.

Owing to its high electron transparency and stability under the electron beam, graphene oxide is also a very promising support film for high resolution structural analysis of macromolecules and nanoparticles by TEM. We have demonstrated this through the analysis of physiological ferritin, both by electron diffraction and high resolution imaging. GO TEM grids are simple, cheap, and quick to fabricate in any laboratory, and as a result could find widespread application in the immediate future.

EXPERIMENTAL SECTION

GO and FLG Preparation. GO was prepared from graphite powder *via* a modified Hummers method[24,25] (see Supporting Information for details). Three different sources of graphite powder were used: Bay Carbon SP-1 graphite powder, and natural graphite flake and powder from the Graphite Trading Company. Each was processed in the same way and gave similar results. First the graphite powder was oxidized: 4.5 g of KNO_3 and 169 mL of concentrated H_2SO_4 were added to 5 g of graphite powder cooling in an ice bath. This mixture was continuously stirred while 22.5 g of $KMnO_4$ was added slowly over 1 h. It was left to stir for a further 2 h in the ice bath, and then removed and left for 5 days, while stirring continuously. After this period a black viscous liquid was obtained; this was added to 500 mL aqueous solution of 5 wt % H_2SO_4 over 1 h, again stirring continuously. After the mixture was stirred for a further 2 h, 15 g of H_2O_2 (30 wt % aqueous solution) was added and then the mixture was left to stir for another 2 h. The oxidized material was then washed. The mixture was added to 500 mL aqueous solution of 3 wt % H_2SO_4, and 0.5 wt % H_2O_2, left to precipitate for 2 days, and then the supernatant was discarded. This was repeated 10 times, resulting in a dark brown slurry. Dispersion of this slurry in water resulted in an aqueous colloidal suspension of graphene oxide. The dispersion and exfoliation of graphite oxide to graphene oxide was aided by mild sonication in an ultrasound bath for 30 min, resulting in a clear, yellow solution. After dispersion there was initially some precipitation, and then the resultant suspension was found to be stable for at least 6 months.

Thin films of GO were fabricated by vacuum filtration onto a 0.22 μm pore size mixed cellulose ester membrane (Millipore). After filtration the membranes were dried in a vacuum desiccator. GO thin films could be removed from the filtration membranes by peeling away the film or by dissolving the membrane in acetone.

Few-layer graphite samples were made using the method described by Hernandez *et al.*;[51] graphite powder was exfoliated by sonication in 1-methyl-2-pyrrolidinone; the dispersion was used immediately after sonication.

Monolayer graphene samples for micro-Raman analysis were prepared by mechanical exfoliation onto silicon oxide as described by Geim *et al.*[52] Monolayer GO samples were prepared by spin-coating GO from a 1 mg mL^{-1} suspension onto silicon oxide. The silicon oxide was cleaned with an oxygen plasma etch immediately prior to coating.

Characterization. Known concentrations of GO were produced by redispersing thin film GO in DI water with the aid of mild son-

ication. Thin film GO samples were also used for X-ray diffraction analysis (XRD), elemental analysis, and TGA. XRD measurements were done on a Panalytical X'Pert Pro MRD, TGA on a Metler-Toledo TGA/DSC1 with a heating rate of 10 °C min^{-1}, and Raman spectroscopy on a Renishaw 1000 spectrometer with 633 nm laser excitation at low power (<0.5 mW) to avoid sample damage. Elemental analysis was done by Warwick Analytical Service.

Electron Microscopy. For TEM analysis a drop of GO/FLG suspension was deposited on a lacey carbon support grid and allowed to dry in air ("drop-casting"). Thin films of GO were also fabricated by vacuum filtration onto a 0.22 μm pore cellulose ester membrane (Millipore), the films were then placed in a sandwich TEM grid for analysis. For accurate quantitative analysis of the GO/FLG lattice spacing, the supporting lacey carbon was sputter coated with Au (thickness 1 to 5 nm) prior to the drop-casting of GO. To test the efficacy of GO as a support grid, horse spleen ferritin (Sigma-Aldrich) was diluted 100:1 in water, and a single drop added to a preprepared GO-coated grid. Low magnification TEM images and selected area electron diffraction (SAED) patterns were obtained at 200 kV on a JEOL 2000FX with a Gatan SC-1000 Orius CCD camera. For SAED a small spot size was used to increase beam coherence, spread into a parallel beam, with a 0.6 μm SA aperture. HR-TEM images of GO were obtained at 80 kV in a JEOL 2010F fitted with a CEOS aberration corrector with the spherical aberration coefficient (*i.e.*, C_3) tuned to +1 μm. HR-TEM images of ferritin on GO were taken at 300 kV on a JEOL JEM-3000F, for which $C_3 = 0.6$ mm. HR-TEM image simulations were carried out using a standard multislice algorithm using parameters typical for our instrument (*i.e.*, coefficient of spherical aberration (C_3) = 0.6 mm, accelerating voltage 300 kV).

Acknowledgment. We thank Ana M. Sanchez for helpful discussions, David Walker and Pam Thomas for XRD, David Hammond for TGA, and Kostya Novoselov for help preparing the graphene samples. PAP thanks the Midland Physics Alliance Graduate School for funding. J.S. is indebted to the Royal Society and to the AIST for financial support and to the Department of Materials, Oxford, for HRTEM facilities accessed through the EPSRC equipment support fund. R.J.Y., I.A.K., and L.G. are grateful for support from the EPSRC through the Manchester/Lancaster Graphene Science and Innovation Award, EP/G035954/1.

Supporting Information Available: S1: Characterization of graphene oxide by AFM and SEM. S2: Graphene oxide *d*-spacing from SAED. S3: Ferritin *d*-spacing from SAED. S4: GO support films directly on copper TEM grid. This material is available free of charge *via* the Internet at http://pubs.acs.org.

REFERENCES AND NOTES

1. Geim, A. K.; Novoselov, K. S. The Rise of Graphene. *Nat. Mater.* **2007**, *6*, 183–191.
2. Ruoff, R. Graphene: Calling All Chemists. *Nat. Nanotechnol.* **2008**, *3*, 10–11.
3. Novoselov, K. S.; Geim, A. K.; Morozov, S. V.; Jiang, D.; Zhang, Y.; Dubonos, S. V.; Grigorieva, I. V.; Firsov, A. A. Electric Field Effect in Atomically Thin Carbon Films. *Science* **2004**, *306*, 666–669.
4. Emtsev, K. V.; Bostwick, A.; Horn, K.; Jobst, J.; Kellogg, G. L.; Ley, L.; McChesney, J. L.; Ohta, T.; Reshanov, S. A.; Rohrl, J.; *et al*. Towards Wafer-Size Graphene Layers by Atmospheric Pressure Graphitization of Silicon Carbide. *Nat. Mater.* **2009**, *8*, 203–207.
5. Kim, K. S.; Zhao, Y.; Jang, H.; Lee, S. Y.; Kim, J. M.; Kim, K. S.; Ahn, J.-H.; Kim, P.; Choi, J.-Y.; Hong, B. H. Large-Scale Pattern Growth of Graphene Films for Stretchable Transparent Electrodes. *Nature* **2009**, *457*, 706–710.
6. Gilje, S.; Han, S.; Wang, M.; Wang, K. L.; Kaner, R. B. A Chemical Route to Graphene for Device Applications. *Nano Lett.* **2007**, *7*, 3394–3398.
7. Gomez-Navarro, C.; Weitz, R. T.; Bittner, A. M.; Scolari, M.; Mews, A.; Burghard, M.; Kern, K. Electronic Transport Properties of Individual Chemically Reduced Graphene Oxide Sheets. *Nano Lett.* **2007**, *7*, 3499–3503.
8. Jung, I.; Dikin, D. A.; Piner, R. D.; Ruoff, R. S. Tunable Electrical Conductivity of Individual Graphene Oxide Sheets Reduced At "Low" Temperatures. *Nano Lett.* **2008**, *8*, 4283–4287.
9. Rao, C. N. R.; Biswas, K.; Subrahmanyam, K. S.; Govindaraj, A. Graphene, the New Nanocarbon. *J. Mater. Chem.* **2009**, *19*, 2457–2469.
10. Ramanathan, T.; Abdala, A. A.; Stankovich, S.; Dikin, D. A.; Herrera Alonso, M.; Piner, R. D.; Adamson, D. H.; Schniepp, H. C.; Chen, X.; Ruoff, R. S.; *et al*. Functionalized Graphene Sheets for Polymer Nanocomposites. *Nat. Nanotechnol.* **2008**, *3*, 327–331.
11. Brodie, B. C. On the Atomic Weight of Graphite. *Philos. Trans. R. Soc.* **1859**, *149*, 10.
12. Mkhoyan, K. A.; Contryman, A. W.; Silcox, J.; Stewart, D. A.; Eda, G.; Mattevi, C.; Miller, S.; Chhowalla, M. Atomic and Electronic Structure of Graphene-Oxide. *Nano Lett.* **2009**, *9*, 1058–1063.
13. Wang, G.; Yang, J.; Park, J.; Gou, X.; Wang, B.; Liu, H.; Yao, J. Facile Synthesis and Characterization of Graphene Nanosheets. *J. Phys. Chem. C* **2008**, *112*, 8192–8195.
14. Paredes, J. I.; Villar-Rodil, S.; Solis-Fernandez, P.; Martinez-Alonso, A.; Tascon, J. M. D. Atomic Force and Scanning Tunneling Microscopy Imaging of Graphene Nanosheets Derived from Graphite Oxide. *Langmuir* **2009**, *25*, 5957–5968.
15. De La Cruz, F. A.; Cowley, J. M. Structure of Graphitic Oxide. *Nature* **1962**, *196*, 468–469.
16. de la Cruz, F. A.; Cowley, J. M. An Electron Diffraction Study of Graphitic Oxide. *Acta Crystallogr.* **1963**, *16*, 531–534.
17. Scholz, W.; Boehm, H. P. Untersuchungen Am Graphitoxid. VI. Betrachtungen Zur Struktur Des Graphitoxids (On Graphite Oxide Investigations. VI. Considerations on the Structure of the Graphite Oxides). *Z. Anorg. Allg. Chem.* **1969**, *369*, 327–340.
18. Jeong, H.-K.; Lee, Y. P.; Lahaye, R. J. W. E.; Park, M.-H.; An, K. H.; Kim, I. J.; Yang, C.-W.; Park, C. Y.; Ruoff, R. S.; Lee, Y. H. Evidence of Graphitic AB Stacking Order of Graphite Oxides. *J. Am. Chem. Soc.* **2008**, *130*, 1362–1366.
19. Nottbohm, C. T.; Beyer, A.; Sologubenko, A. S.; Ennen, I.; Hütten, A.; Rösner, H.; Eck, W.; Mayer, J.; Gölzhäuser, A. Novel Carbon Nanosheets as Support for Ultrahigh-Resolution Structural Analysis of Nanoparticles. *Ultramicroscopy* **2008**, *108*, 885–892.
20. Booth, T. J.; Blake, P.; Nair, R. R.; Jiang, D.; Hill, E. W.; Bangert, U.; Bleloch, A.; Gass, M.; Novoselov, K. S.; Katsnelson, M. I.; Geim, A. K. Macroscopic Graphene Membranes and Their Extraordinary Stiffness. *Nano Lett.* **2008**, *8*, 2442–2446.
21. Meyer, J. C.; Girit, C. O.; Crommie, M. F.; Zettl, A. Imaging and Dynamics of Light Atoms and Molecules on Graphene. *Nature* **2008**, *454*, 319–322.
22. Meyer, J. C.; Girit, C. O.; Crommie, M. F.; Zettl, A. Hydrocarbon Lithography on Graphene Membranes. *Appl. Phys. Lett.* **2008**, *92*, 123110–3.
23. Meyer, J. C.; Kisielowski, C.; Erni, R.; Rossell, M. D.; Crommie, M. F.; Zettl, A. Direct Imaging of Lattice Atoms and Topological Defects in Graphene Membranes. *Nano Lett.* **2008**, *8*, 3582–3586.
24. Eda, G.; Fanchini, G.; Chhowalla, M. Large-Area Ultrathin Films of Reduced Graphene Oxide as a Transparent and Flexible Electronic Material. *Nat. Nanotechnol.* **2008**, *3*, 270–274.
25. Hummers, W. S.; Offeman, R. E. Preparation of Graphitic Oxide. *J. Am. Chem. Soc.* **1958**, *80*, 1339.
26. Szabo, T.; Berkesi, O.; Forgo, P.; Josepovits, K.; Sanakis, Y.; Petridis, D.; Dekany, I. Evolution of Surface Functional Groups in a Series of Progressively Oxidized Graphite Oxides. *Chem. Mater.* **2006**, *18*, 2740–2749.
27. Pimenta, M. A.; Dresselhaus, G.; Dresselhaus, M. S.; Cancado, L. G.; Jorio, A.; Saito, R. Studying Disorder in Graphite-Based Systems by Raman Spectroscopy. *Phys. Chem. Chem. Phys.* **2007**, *9*, 1276–1290.

28. Kudin, K. N.; Ozbas, B.; Schniepp, H. C.; Prud'homme, R. K.; Aksay, I. A.; Car, R. Raman Spectra of Graphite Oxide and Functionalized Graphene Sheets. *Nano Lett.* **2008**, *8*, 36–41.
29. The size of the sheets observed by TEM ranged from ~100 nm across, to sheets larger than 10 μm in both dimensions. This was consistent with AFM and FE-SEM measurements (see Supporting Information).
30. Meyer, J. C.; Geim, A. K.; Katsnelson, M. I.; Novoselov, K. S.; Obergfell, D.; Roth, S.; Girit, C.; Zettl, A. On the Roughness of Single- and Bi-Layer Graphene Membranes. *Solid State Commun.* **2007**, *143*, 101–109.
31. Horiuchi, S.; Gotou, T.; Fujiwara, M.; Asaka, T.; Yokosawa, T.; Matsui, Y. Single Graphene Sheet Detected in a Carbon Nanofilm. *Appl. Phys. Lett.* **2004**, *84*, 2403–2405.
32. Horiuchi, S.; Gotou, T.; Fujiwara, M.; Sotoaka, R.; Hirata, M.; Kimoto, K.; Asaka, T.; Yokosawa, T.; Matsui, Y.; Watanabe, K.; Sekita, M. Carbon Nanofilm with a New Structure and Property. *Jpn. J. Appl. Phys.* **2003**, *42*, L1073.
33. Luo, Z.; Lu, Y.; Somers, L. A.; Johnson, A. T. C. High Yield Preparation of Macroscopic Graphene Oxide Membranes. *J. Am. Chem. Soc.* **2009**, *131*, 898–899.
34. Liu, Z.; Suenaga, K.; Harris, P. J. F.; Iijima, S. Open and Closed Edges of Graphene Layers. *Phys. Rev. Lett.* **2009**, *102*, 015501−4.
35. Warner, J. H.; Rummeli, M. H.; Gemming, T.; Buchner, B.; Briggs, G. A. D. Direct Imaging of Rotational Stacking Faults in Few-Layer Graphene. *Nano Lett.* **2009**, *9*, 102–106.
36. For a two-dimensional material electron diffraction measures the separation between atoms projected into the plane perpendicular to the electron beam. Here the beam is perpendicular to the specimen.
37. Elias, D. C.; Nair, R. R.; Mohiuddin, T. M. G.; Morozov, S. V.; Blake, P.; Halsall, M. P.; Ferrari, A. C.; Boukhvalov, D. W.; Katsnelson, M. I.; Geim, A. K.; Novoselov, K. S. Control of Graphene's Properties by Reversible Hydrogenation: Evidence for Graphane. *Science* **2009**, *323*, 610–613.
38. Boukhvalov, D. W.; Katsnelson, M. I. Modeling of Graphite Oxide. *J. Am. Chem. Soc.* **2008**, *130*, 10697–10701.
39. Zobelli, A.; Gloter, A.; Ewels, C. P.; Seifert, G.; Colliex, C. Electron Knock-on Cross Section of Carbon and Boron Nitride Nanotubes. *Phys. Rev. B* **2007**, *75*, 245402–9.
40. Gass, M. H.; Bangert, U.; Bleloch, A. L.; Wang, P.; Nair, R. R.; Geim, A. K. Free-Standing Graphene at Atomic Resolution. *Nat. Nanotechnol.* **2008**, *3*, 676–681.
41. Swift, P. Adventitious Carbon—the Panacea for Energy Referencing. *Surf. Interface Anal.* **1982**, *4*, 47–51.
42. Massover, W. H. Ultrastructure of Ferritin and Apoferritin: A Review. *Micron* **1993**, *24*, 389–437.
43. Iijima, S. Thin Graphite Support Films for High Resolution Electron Microscopy. *Micron* **1977**, *8*, 41–46.
44. Quintana, C.; Cowley, J. M.; Marhic, C. Electron Nanodiffraction and High-Resolution Electron Microscopy Studies of the Structure and Composition of Physiological and Pathological Ferritin. *J. Struct. Biol.* **2004**, *147*, 166–178.
45. Michel, F. M.; Ehm, L.; Antao, S. M.; Lee, P. L.; Chupas, P. J.; Liu, G.; Strongin, D. R.; Schoonen, M. A. A.; Phillips, B. L.; Parise, J. B. The Structure of Ferrihydrite, a Nanocrystalline Material. *Science* **2007**, *316*, 1726–1729.
46. Jansen, E.; Kyek, A.; Schäfer, W.; Schwertmann, U. The Structure of Six-Line Ferrihydrite. *Appl. Phys. A: Mater. Sci. Process.* **2002**, *74*, s1004–s1006.
47. Galvez, N.; Fernandez, B.; Sanchez, P.; Cuesta, R.; Ceolin, M.; Clemente-Leon, M.; Trasobares, S.; Lopez-Haro, M.; Calvino, J. J.; Stephan, O.; Dominguez-Vera, J. M. Comparative Structural and Chemical Studies of Ferritin Cores with Gradual Removal of Their Iron Contents. *J. Am. Chem. Soc.* **2008**, *130*, 8062–8068.
48. A graphene lattice is simulated rather than GO as the exact structure of GO is not known. The difference in contrast between GO and graphene is negligible when compared to the contrast due to the ferritin.
49. Relative to the trigonal $P\bar{3}1c$ ferrihydrite model the nanoparticle is oriented along [001] with respect to the electron beam direction.
50. Ferritin particles are randomly orientated on the GO support, with correspondingly random orientations of the core structure. These particles are presented as they happen to lie orientated along a crystallographic axis.
51. Hernandez, Y.; Nicolosi, V.; Lotya, M.; Blighe, F. M.; Sun, Z.; De, S.; McGovern, I. T.; Holland, B.; Byrne, M.; Gun'Ko, Y. K.; *et al*. High-Yield Production of Graphene by Liquid-Phase Exfoliation of Graphite. *Nat. Nanotechnol.* **2008**, *3*, 563–568.
52. Geim, A. K.; Kim, P. Carbon Wonderland. *Sci. Am.* **2008**, *298*, 90–97.